A secondary zone of uplift measured after megathrust earthquakes: caused by early downdip afterslip?

Théa Ragon[1], Mark Simons[1]

[1]Seismological Laboratory, California Institute of Technology, Pasadena, CA, USA.

Key Points:

- After large subduction earthquakes, a secondary zone of uplift (SZU) is measured several hundred kilometers from the trench
- The SZU is not reproduced by coseismic finite-fault models that neglect 3D elastic heterogeneities in lithospheric structure
- The SZU is reproduced using plausible models of 3D elastic heterogeneities, with slip downdip of the main coseismic patch

Corresponding author: Théa Ragon, `tragon@caltech.edu`

Abstract

A secondary zone of surface uplift (SZU), located ∼300 kilometers landward of the trench, has been measured after several megathrust earthquakes. The SZU reached a few centimeters hours to days after the 2011 M_w 9.1 Tohoku (Japan) and 2010 M_w 8.8 Maule (Chile) earthquakes. Published coseismic finite-fault models for these events do not reproduce the measured SZU. One interpretation is that this SZU is universal, driven by volume deformation around the slab interface (van Dinther et al. 2019). In contrast, we demonstrate the SZU may instead result from slip on the slab interface. Further, we suggest the SZU could be caused by rapid postseismic afterslip. We can reproduce the SZU with fault slip if elastic heterogeneities associated with the subducting slab are accounted for, as opposed to assuming homogeneous or layered elastic lithospheric structures.

Plain Language Summary

Large earthquakes in subduction zones induce displacement of the ground surface, which usually include large amplitude uplift offshore, transitioning to a mild region of subsidence further inland. After the largest instrumented earthquakes, such as the 2011 M_w 9.1 Tohoku (Japan), the 1960 M_w 9.5 Valdivia (Chile) and 1964 M_w 9.2 Alaska earthquakes, a secondary zone of uplift (SZU) is detectable even further inland. The origin of this SZU remains enigmatic, but one interpretation is that it derives from deformation of the volume around the subducting fault (van Dinther et al. 2019). In this study, we investigate alternate interpretations of its origin. A simple slip model with realistic variations in crustal elastic properties allows one to reproduce the secondary zone of uplift. We then focus on the 2010 M_w 8.8 Maule (Chile) event, for which some measures of the SZU peaked at 12 cm. Unlike previously published studies, we can reproduce the SZU with on-fault displacement, located significantly deeper than the region of estimated coseismic slip. This deep slip likely occurred in the hours after the earthquake.

1 Introduction

Simple models of subduction zone thrust earthquakes based on a single dip-slip dislocation embedded in an elastic half space produce a large surface uplift in near field, and a zone of small amplitude subsidence that slowly tapers to zero in the far field (Fig. 1a, primary slip patch, e.g., Savage, 1983). Vertical displacements measured after most subduction earthquakes follow a similar pattern. However, some far field geodetic measurements of megathrusts earthquakes ($M_w > 8$) detect a coseismic secondary zone of uplift (referred to as SZU in the text) a few hundred kilometers landward of the trench (for a summary, see van Dinther et al., 2019). In the years following the 1960 M_w 9.5 Valdivia and 1964 M_w 9.2 Alaska earthquakes (e.g., Plafker & Savage, 1970; Kanamori, 1970), uplifts of more than 1 m and 30 cm in amplitude, respectively, were measured in this secondary zone. After the 2010 M_w 8.8 Maule and 2011 M_w 9.0 Tohoku earthquakes, a few centimeters of secondary uplift were recorded in some datasets in the days to weeks following the mainshock. For the Maule event, the SZU has been measured by survey Global Navigation Satellite Systems (GNSS) and is not observed on other datasets (continuous GNSS, or Interferometric Synthetic Aperture Radar, InSAR, e.g., Vigny et al., 2011; Xiong et al., 2022, Fig. 1c). For the Tohoku earthquake, continuous GNSS, and possibly InSAR, recorded the SZU (e.g., Ozawa et al., 2011; Hu et al., 2013). Whether this uplift is coseismic or rapid postseismic is unknown at this time.

The origin and consistency of the SZU remains ambiguous. None of the published coseismic slip models of the 2010 Maule event reproduce simultaneously the horizontal deformation, the near-field vertical displacements and the SZU (Fig. 1c shows a selec-

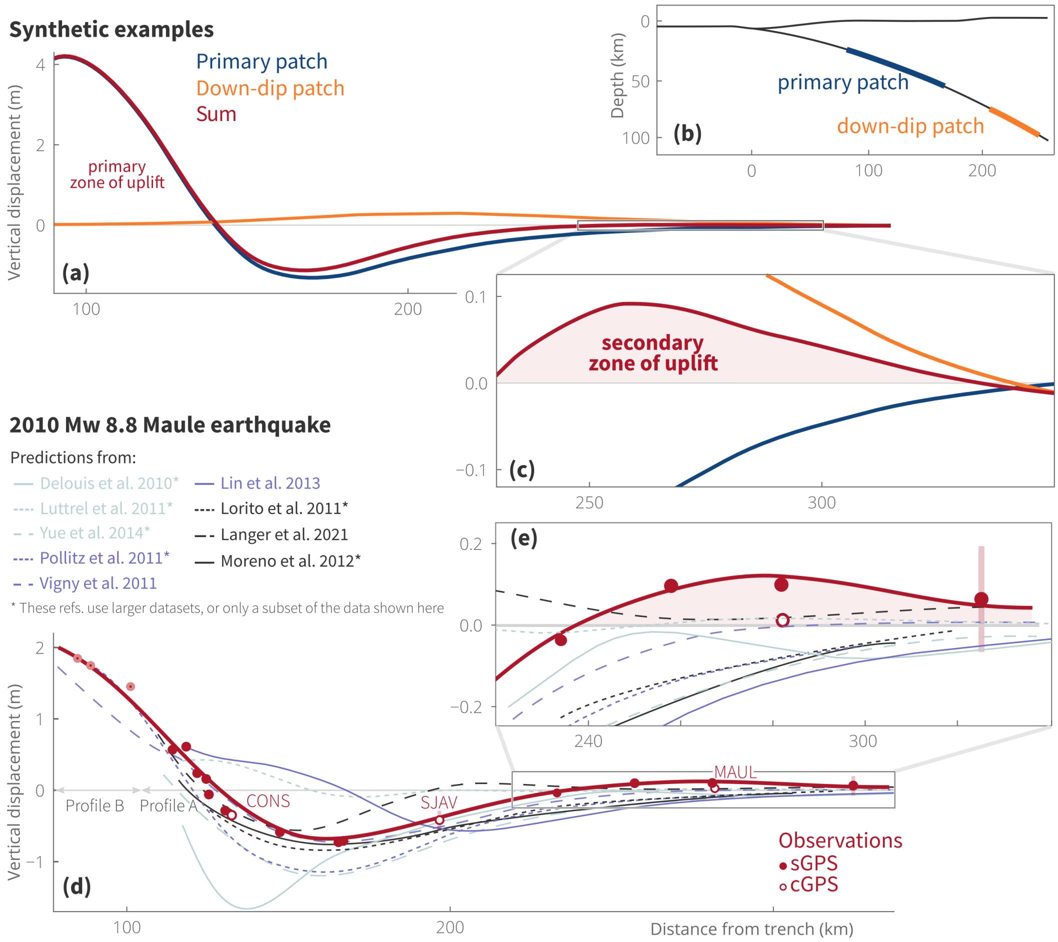

Figure 1. Synthetic and observed trench perpendicular profiles of vertical surface displacements. (a) Vertical surface displacement induced by a ∼40-km-deep primary slip patch, by a secondary downdip patch (∼ 90-km-depth), and the sum of the two. The zoomed inset (c) shows that the sum of these two patches induces a ∼10 cm secondary zone of uplift ∼250 km from the trench. (b) Cross section of the synthetic subduction zone, with the location of the primary and downdip slip patches. (d) Co-seismic static vertical displacement measured by survey and continuous GNSS for the 2010 M_w 8.8 Maule earthquake for profile A (3 near-trench points are from profile B to mimic (a)), and predictions from several published models. Location of the profiles are in Figs S1 and 5, data from Vigny et al. (2011). The name of cGNSS stations is indicated. Note that at cGNSS station MAUL, only 5 mm of uplift has been measured. (e) The zoomed inset shows the inability of published finite fault slip models to explain the measured secondary zone of uplift. Predictions from Delouis et al. (2010); Luttrell et al. (2011); Pollitz et al. (2011); Lin et al. (2013) have been produced using models from the SRCMOD database (Mai & Thingbaijam, 2014); others have been reproduced from published material (Yue et al., 2014; Lorito et al., 2011; Langer et al., 2020; Moreno et al., 2012). Note that these models were derived using different datasets (sometimes including only a subset of the data shown here). Location of the profile, data and other trench-perpendicular profiles are shown in Fig. S1. Vertical bars indicate measurement errors, which are often of ∼10-20 mm and therefore smaller than the size of the dot.

tion of published slip models, see enclosed references). Similarly, none of the published coseismic slip models for the 2011 Tohoku earthquake explain the observed SZU (e.g., Lay, 2017), whose amplitude is less than a twentieth of the near-field vertical displacement. Note that, for these two events, >1-year-postseismic SZU can be modeled with afterslip or viscoelastic processes (e.g., Klein et al., 2016; Ichimura et al., 2016; Li et al., 2017; Agata et al., 2019; Peña et al., 2020). But classic elastic dislocation or elastic/viscoelastic rebound models fail to predict any coseismic SZU (van Dinther et al., 2019). van Dinther et al. (2019) propose that the SZU is universal, coseismic, and that is is the result of an elastic rebound of the lithosphere and an upward elastic flow in the mantle wedge.

While a single patch of fault slip cannot produce a SZU at the surface, an additional downdip patch potentially can (Fig. 1a). We should expect that a finite-fault model could infer a downdip slip patch to explain any observed SZU. However, existing published slip models do not.

In the following, we investigate under which assumptions the SZU can, or cannot, be predicted with fault slip. We begin by considering that the SZU is coseismic by default. We explore the effect of assuming homogeneous crustal velocities or a stiffer subducting slab, and more compliant forearc, on predicted surface displacements. We first investigate the effect of 3D elastic heterogeneities for a synthetic subduction case. Then, we focus on the Maule event, for which the SZU likely reaches a few cm and could not be reproduced (Fig 1c) even with added complexity in crustal properties: curved and deeper slab geometries, topography, heterogeneous crustal elastic properties, etc (Lin et al., 2013; Moreno et al., 2012; Langer et al., 2020). While we do not discard the possibility that the SZU might be affected by deformation of the volume around the slab interface, we show it may simply be the result of slip on this interface. We end with a discussion of the geodetic datasets that have recorded the SZU for the the 2010 M_w 8.8 Maule and 2011 M_w 9.0 Tohoku earthquakes, and discuss the timing of the SZU relative to the mainshocks.

2 A synthetic example: secondary zone of uplift caused by downdip slip

We begin by designing a synthetic subduction zone, where the lithosphere is divided in domains of different elastic properties, generic trench-perpendicular topographic variations and a curved slab interface whose architecture varies slightly along strike (Fig. 2f). This subduction zone is characterized by a stiff plunging slab overlain by a compliant oceanic crust; the continental domain consists of a 35-km-thick crust, more compliant than the underlying mantle whose density increases with depth (domain properties detailed in Suppl. Mat. Text S2, Tab. S1, Figs S2, S3). We apply slip on a limited region of the slab interface (Fig. 1b). Because of the inhomogeneous elastic structure, we rely on a finite element approach (Pylith, Aagaard et al., 2013) to calculate surface displacements.

We first compare the strain produced by a ∼40-km-deep slip patch on the assumed fault, embedded either in a model with 3D variations of elastic properties or with a layered crust (Fig. 2). The layered crust replicates the continental domain of its 3D counterpart and does not incorporate variations in topography (Fig. 2g). Relative to the layered elastic models, the 3D-heterogeneous models produce a primary zone of subsidence (150-200 km from the trench) that is smaller in amplitude and tapers to zero closer to the trench. In the region of primary subsidence, the impact of elastic heterogeneity is ∼5 times larger for vertical displacements than for horizontal ones (Figs 2, S4, 25% of peak amplitude versus 5% respectively).

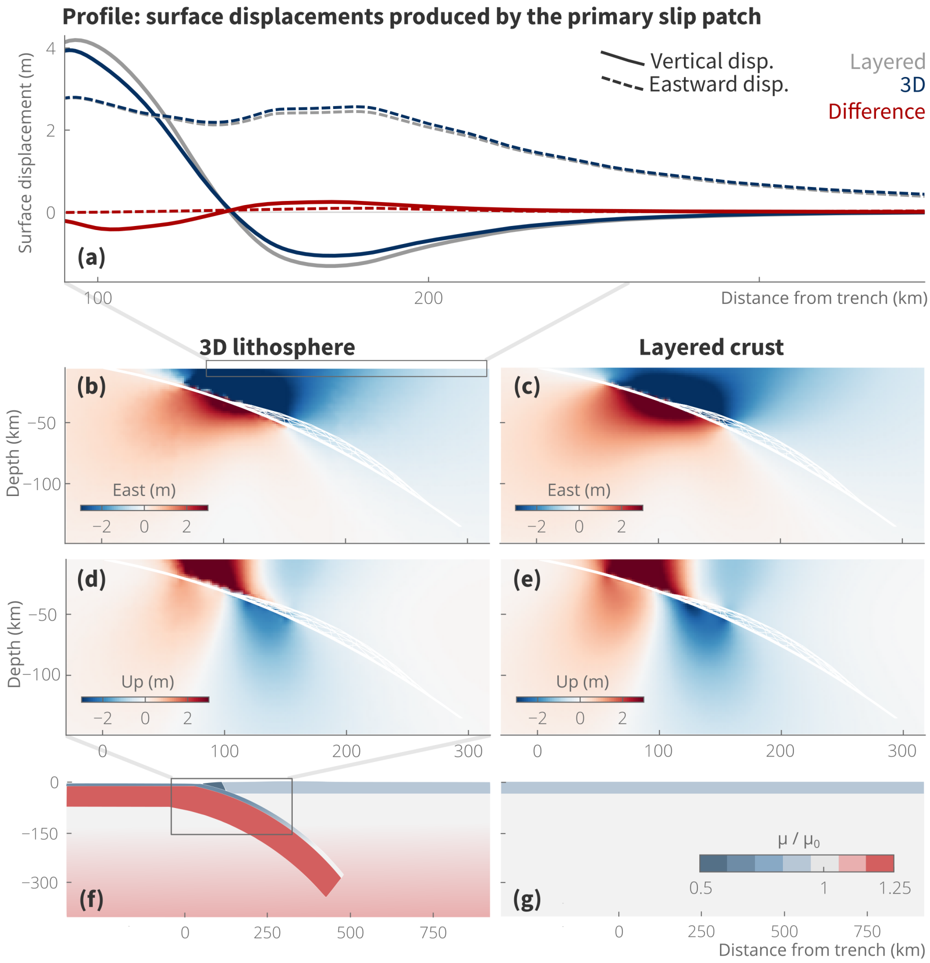

Figure 2. Displacements produced by a ∼40-km-deep slip patch on a slab embedded in a 3D lithosphere or a layered crust. (a) Trench-perpendicular profiles of surface displacements. (b,d) and (c,e) Trench-perpendicular cross-sections of upward and eastward displacements for the elastic properties shown in (f) and (g), respectively.

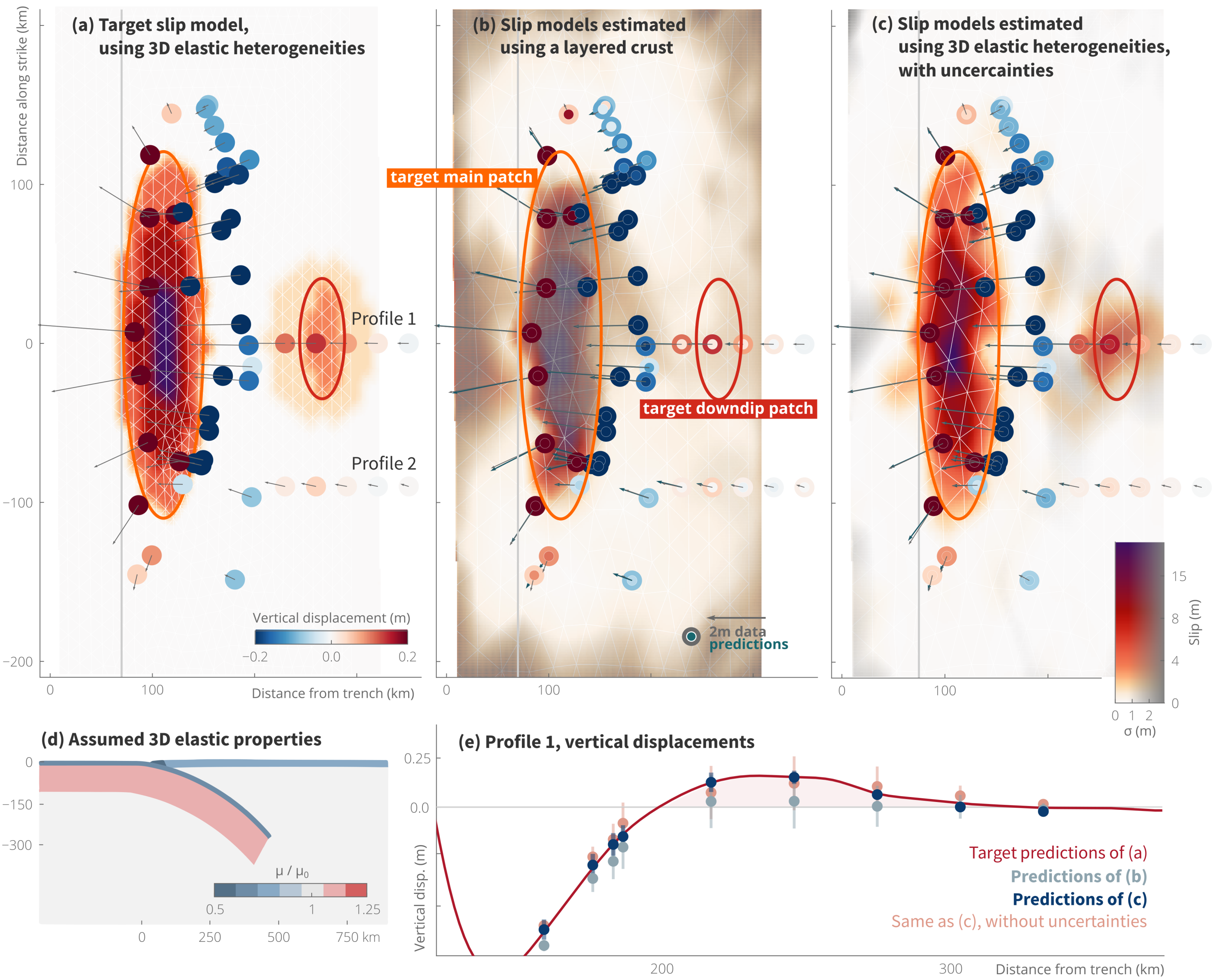

Figure 3. Synthetic example: (a) Target slip and surface displacements. (b,c) Inferred slip and surface displacement assuming incorrect lithospheric structure, either with a layered crust (b) or with 3D-varying elastic properties, shown in (d). Gray shading is the standard deviation of the inferred slip (Fig. S5). In (b) and (c), the assumed fault replicates the true geometry shown in (a), but extends to greater depths. In (c), uncertainties in elastic properties are accounted for: Note the difference in the spatial distribution of posterior uncertainties. (d) Assumed 3D elastic properties, μ_0=52 GPa, which differ from the properties used to calculate synthetic observations (displayed in Fig. 2f). (e) Trench perpendicular profile of the target synthetic data and predicted vertical displacements (at 0-km-along-strike). Vertical error bars indicate the posterior uncertainty. Predictions in light red are for the model shown in Fig. S9.

We then assume two slip patches, the primary patch peaks at 17 m of slip while the secondary downdip patch has 3.5 m of slip (Fig. 1b). We here consider every slip is coseismic. With the heterogeneous elastic model, we calculate the induced displacement offsets at 50 locations randomly distributed at the surface, to which we add two E-W profiles. The profiles mimic the spatial distribution of the GNSS data of the Maule event (Fig S1, Vigny et al., 2011). Induced displacements reproduce the ∼15-cm-uplift measured 250-300 km away from the trench after the Maule earthquake (Figs 1a and d, S1). We add white and spatially correlated noise to these synthetic data, and try to recover the target slip patches assuming the correct fault geometry (with larger subfaults) and an elastic structure that is different from the one used to calculate synthetic surface displacements. The assumed structure is either layered (Fig. 2g), or with 3D variations (Fig. 3d). We use a Bayesian sampling approach to infer fault slip from the synthetic displacement (detailed in Suppl. Mat. section S1, Minson et al., 2013).

When the crust is assumed layered (or homogeneous), the secondary uplift cannot be fit (and is not within posterior uncertainty, Fig. 3a,c, Fig. S6, respectively). Relative to the model with heterogeneous elastic properties, a layered crust produces wider and larger primary zone of subsidence, while the horizontal displacements are only slightly impacted (Fig. 2). The amount of slip required to explain the horizontal displacements is incompatible with the slip required to explain the vertical ones. Most inversions typically favor fitting the horizontal measurements, since they are larger and usually more certain. Some downdip slip is imaged, as required by the horizontal displacements, if the fault is deep enough. Assuming a fault model that is too shallow, and/or subject to unphysical spatial smoothing, can prevent resolution of the downdip patch (Fig. S7). The SZU can be produced with incorrect inferred slip, and to the detriment of the fit to the horizontal displacements, if assuming very low measurement errors for the vertical displacements only (1 mm, i.e. very strongly favoring their fit) and a fault geometry that extends to great depths (Fig. S8).

In contrast, adopting a relatively realistic crustal structure (e.g., with 3D heterogeneities in elastic properties for a typical subduction zone, even if the properties are imperfectly known, detailed in Tab. S2), allows one to reproduce the SZU, and to recover the downdip slip patch (Fig. 3b,c). Accounting for uncertainties in elastic properties (following the methodology presented in Ragon & Simons, 2021, Fig. 3c,d) improves the fit to the data. The main annoyance in assuming heterogeneous crustal elastic properties for slip inference is the computational burden. With this simple synthetic example, we show that a SZU can be produced by downdip slip on the slab interface by accounting for 3D variations in elastic properties.

3 Recovering the secondary uplift of the 2010 M_w 8.8 Maule earthquake

The results of our synthetic example suggest that assuming a realistic crustal structure when imaging coseismic slip for the Maule and Tohoku earthquakes may allow one to reproduce the measured SZU. We choose to explore the 2010 Chile earthquake, as the measured SZU shows a larger amplitude that should be easier to reproduce. It is important to note that the SZU for the Maule event only shows on survey GNSS measurements (Vigny et al., 2011, Fig. 1), and is very mild ot not discernible on continuous GNSS (5 mm uplift at station MAUL, Fig. 1) or InSAR data (e.g., Xiong et al., 2022). In this section, we assume the observed SZU is real, but we discuss this assumption in section 4. We solve for the slip distribution and amplitude using the GNSS data from Vigny et al. (2011), completed by a few far field data from Lin et al. (2013).

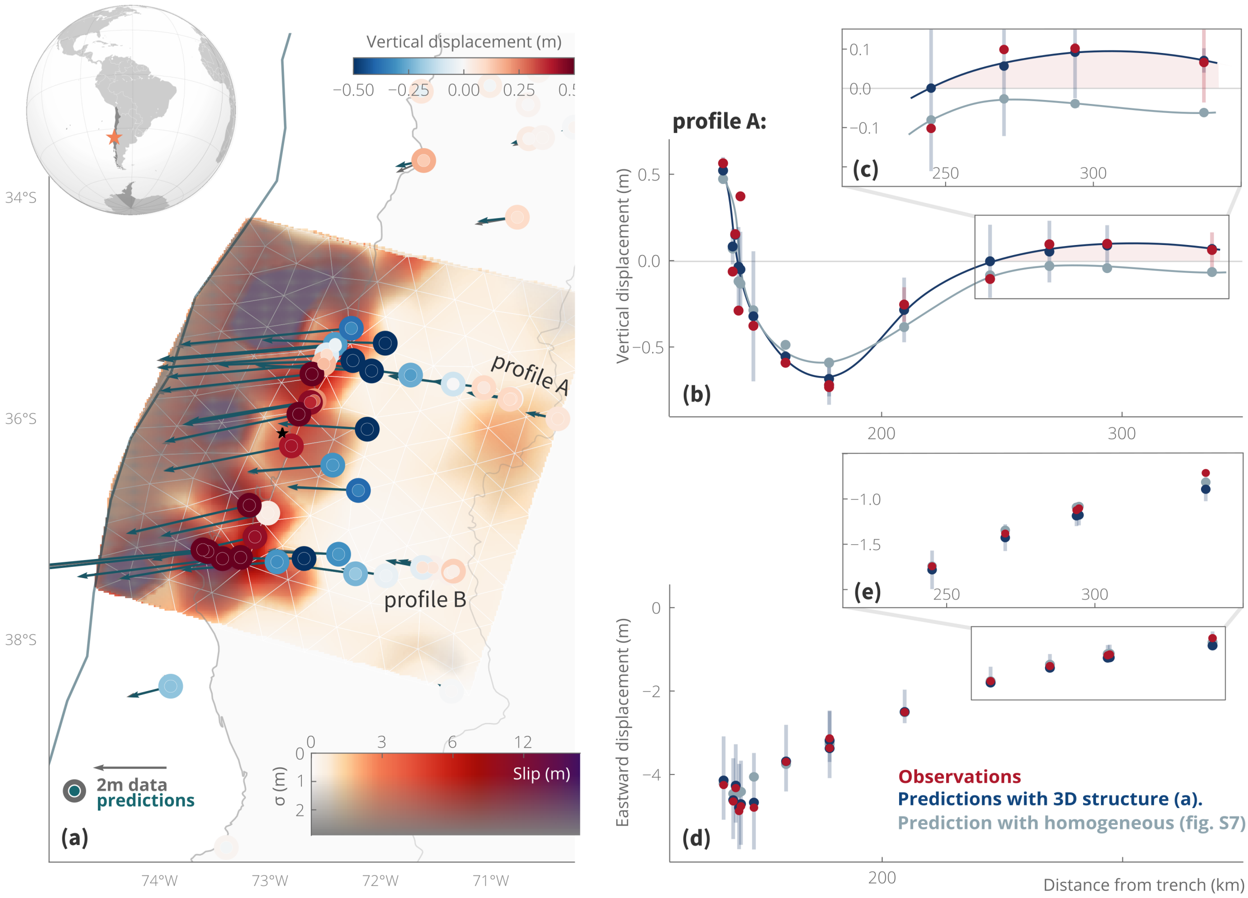

Figure 4. The 2010 M_w 8.8 Maule earthquake: (a) inferred coseismic slip model as well as observed and predicted surface displacements, assuming a 3D crustal structure and accounting for related epistemic uncertainties. Grey shading indicates the standard deviation of the inferred slip (Fig. S15). (b) Trench perpendicular profile (profile A) of measured and predicted vertical displacements (without data at MAUL station), for the slip model shown in (a), and a slip model inferred assuming an homogeneous crustal structure (Fig. S12). Vertical error bars indicate the posterior uncertainty and data errors. (d) Same as (b) for eastward surface displacements. (c) and (e) Zoomed inset on the SZU region.

We build a realistic crustal model for the calculation of the Green's functions (Figs S10, S11, slab geometry from Slab2, elastic properties from LITHO1.0, topography from ETOPO1, Hayes et al., 2018; Pasyanos et al., 2014; NCEI, 2008). While more detailed velocity models and datasets are available, our goal is to explore the secondary uplift, not to image the slip in detail. We also account for potential uncertainties in the assumed fault geometry and elastic properties (following the methodology presented in Ragon & Simons, 2021). Uncertainties in fault geometry are calculated by varying the dip of the assumed slab geometry while keeping the location of the trench and elastic properties fixed. Note that changing the fault geometry to fit the SZU has already been attempted by several authors (Lin et al., 2013; Langer et al., 2020), without success, and therefore the uncertainties in fault geometry have a limited role to play here.

The inferred slip model reproduces the SZU (Fig. 4). We image a primary zone of fault slip in most of the offshore region, with a large uncertainty of 2-to-4 m in average (and up to 10 m in the near-trench domain, Fig. S15). Downdip of this primary region of slip, at ∼90-km-depth, we infer a well-constrained slip zone with an amplitude of 2.5-3 m, equivalent to M_w=7.2, which is responsible for the secondary uplift. Models assuming a layered or homogeneous crust do not image this downdip slip and do not reproduce the SZU (Fig. 1c and enclosed references, Figs S12, S13, S14). Models assuming an heterogeneous elastic structure, but neglecting related epistemic uncertainties, are able to reproduce the SZU albeit not as well as when epistemic uncertainties are accounted for (Figs S13, S14).

Our results suggest that previously published models for the Maule earthquake were not able to reproduce the SZU (Fig. 1c) because most of them were inferred assuming a layered crust. While Moreno et al. (2012) assumed 3D heterogeneous elastic properties, the shallow fault geometry they used and the impact of spatial regularization likely prevented a downdip patch to be imaged. Note that some authors do infer downdip slip as required by horizontal displacements (e.g., Delouis et al., 2010; Vigny et al., 2011; Bedford et al., 2013; Yue et al., 2014), but that the inferred slip could not cause a SZU for the same reasons (as shown in our synthetic example, Fig. 3a). The combined effect of strong assumptions on the crustal elastic structure and fault geometry, and the common use of unphysical regularization (e.g., Ortega-Culaciati et al., 2021), probably prevented published models from producing the mild secondary uplift of the Tohoku earthquake (while, similarly to the Maule earthquake, some authors do infer downdip slip as required by horizontal displacement, e.g., Periollat et al., 2022).

4 What is the secondary zone of uplift?

That we image downdip slip does not mean slip is uniquely the cause of the SZU. Challenges in modeling highly disparate time-scales (from seconds to years) prevent van Dinther et al. (2019) from confirming the universal process they invoke is coseismic, rather than lasting several weeks after the mainshock. In contrast, while the potential influence of volume deformation cannot be ruled out, the hypothesis that downdip slip caused the SZU seems straightforward. For the 2010 Maule earthquake, we infer downdip slip at ∼90-km-depth, where only a few aftershocks occurred, none with $M_w > 6$ (Rietbrock et al., 2012; Lange et al., 2012). Such depths are generally believed to be relatively aseismic (Lay et al., 2012; Obara & Kato, 2016). Moreover, in south-central Chile intermediate-depth seismicity is relatively sparse (Fig. 5 Ruiz & Madariaga, 2018) We conclude that the downdip slip we image (equivalent M_w=7.2) is likely aseismic in nature, and therefore postseismic.

The SZU observed after megathrust earthquakes other than the Maule event is located 300 km from the trench in Chile, 350 km in Japan, and 400 km in Alaska (van Dinther et al., 2019). Assuming that the SZU finds its origin in slip downdip of the

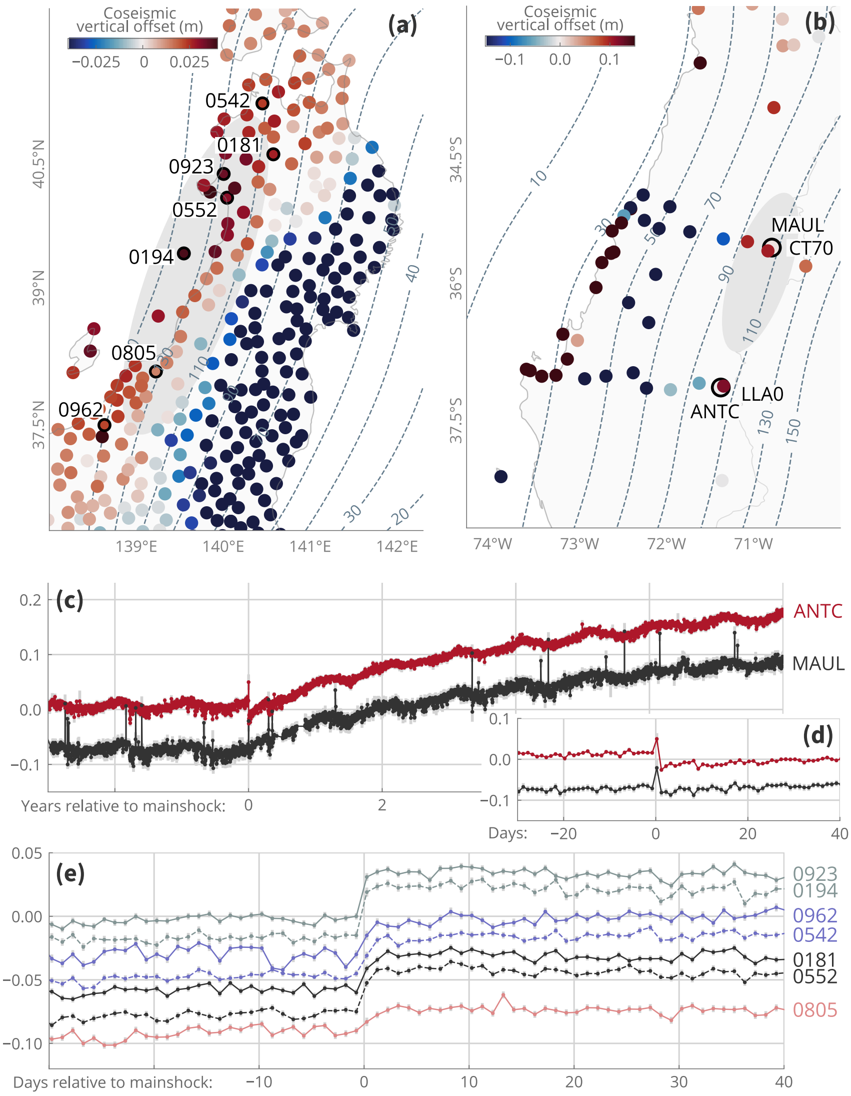

Figure 5. GNSS coseismic vertical offsets (a,b) and times series (c,d,e) for the 2011 M_w 9.1 Tohoku (Japan, a,e) and the 2010 M_w 8.8 Maule (Chile) earthquakes (b,c,d). The gray area corresponds to the location of the potential rapid afterslip at the origin of the SZU. (a) Daily coseismic vertical offsets calculated from non-detrended time series (processed by Periollat et al., 2022). (b) Coseismic vertical offsets from survey GNSS or daily solutions (from Vigny et al., 2011). Continuous GNSS stations MAUL and ANTC are circled in black. Slab depths contours are overlayed. (c) Detrended vertical daily time series (meters) at the SZU location (from Klein et al., 2022); (d) is a zoomed inset around the mainshock. (e) Non-detrended daily vertical time series (meters) at selected locations in the SZU (from Periollat et al., 2022). For (c), (d) and (e), standard deviation is plotted as a vertical gray bar.

coseismic rupture, because of the various slab geometries, the downdip slip would have consistently occurred at ∼90-120-km-depth. Following the same arguments as for the Maule earthquake,, the slip that caused the SZU would therefore be postseismic. For the 1960 M_w 9.5 Valdivia and 1964 M_w 9.2 Alaska earthquakes, leveling data measured a few months to years after the mainshocks will probably contain a large postseismic component (e.g., Plafker & Savage, 1970; Plafker, 1965; van Dinther et al., 2019). In contrast, that coseismic geodetic data for the Maule and Tohoku earthquakes recorded the SZU would suggest it has been produced by early afterslip (hours to weeks after the mainshock), signal of which is often included in coseismic geodetic offsets.

For the Maule earthquake, the SZU is only recorded by survey GNSS, which were acquired several days to weeks after the mainshock (Vigny et al., 2011, same reference for coseismic data description below), and therefore contain some postseismic signal. 3D displacement fields extracted from InSAR data also contain some postseismic deformation and show, in the SZU location, from -50 to +20 cm of vertical offset depending on the approach used (Xiong et al., 2022); and are therefore not reliable to investigate the SZU. At two continuous stations located in the region of the SZU (MAUL and ANTC, Fig. 5), coseismic vertical offset measured from the difference of positions the day before and after the mainshock is of 5±9 and -16±11 mm, respectively. Estimated offsets at collocated survey stations (CT70 and LLA0, Fig. 5) reach 102±14 and 120±13 mm. Such difference would indeed suggest that the ∼10 cm SZU has been caused by afterslip in the weeks following the mainshock. However, daily time-series estimated at the same continuous GNSS station do need two years to reach 10 cm uplift (MAUL and ANTC, Fig. 5, Klein et al., 2022).

Unlike continuous GNSS data, coseismic survey offsets published by Vigny et al. (2011) were calculated by extrapolating interseismic velocities over 10 years. Interseismic velocity estimates have been derived from the few measurements available (only 3 data points in 1996, 1999 and 2002, e.g., Ruegg et al., 2009). Additionally, daily time series at MAUL and ANTC (Fig. 5) show non-negligible seasonal variations (>20 mm in amplitude), that have likely altered the sparse interseismic velocity measurements. At the SZU location, the combination of small and uncertain interseismic rates with small coseismic amplitudes thus makes the errors on survey vertical offsets larger than those on continuous data.

The large data errors on survey GNSS vertical offsets and the sparsity of continuous GNSS data make the apparent contradiction between estimated offsets difficult to resolve. This contradiction further suggests that the SZU did not reach 10 cm in amplitude in the few days to months after the mainshock. However, the possibility of a few cm rapid postseismic SZU in the hours following the mainshock cannot be discarded without a detailed analysis of times series with a rate higher than 1 day (Fig. 5d).

For the Tohoku earthquake, up to 44±20 mm of uplift in the SZU location (Ozawa et al., 2011) is measured for offsets estimated by subtracting the average positions for the period between 2 days and 6 hours before the mainshock from the positions 3 hours after the mainshock. Early afterslip offsets, estimated from the difference between positions 3 hours before and 14 days after the mainshock by Ozawa et al. (2011) show up to 50±20 mm uplift in the far field, but not necessarily at the same locations as the coseismic offsets. Periollat et al. (2022) processed daily time series that also show up to 45±5 mm uplift in the 1 to 3 days following the mainshock (Fig. 5). While some daily positions could suggest a 3-days transient postseismic uplift (Fig. 5), the vertical component of their 30-s time series has a poor signal to noise ratio and cannot be exploited. Finally, 3D displacement field derived from InSAR data do reproduce some far-field uplift, but is not independent from measured GNSS offsets (Hu et al., 2013).

We demonstrate that the SZU is likely caused by downdip afterslip happening in the hours following the mainshock. While, for the Maule earthquake, the SZU remains ambiguous as only two continuous GNSS stations might have recorded the corresponding signal, the SZU is clearly measured in the days after the Tohoku earthquake. Any further conclusion cannot be made without a thorough examination of early postseismic GNSS time series, what is beyond the scope of this study.

5 Discussion and conclusion

A secondary zone of uplift (SZU) has been observed after several megathrust earthquakes. In this study, we investigate if (and which) assumptions in the foward and/or inverse approach could prevent the SZU to be reproduced with slip on the slab interface. We show that neglecting variations in elastic properties due to the plunging slab induces an incompatibility in the amount of slip required to explain the measured horizontal, or vertical, displacements, preventing models from reproducing the SZU. In contrast, we demonstrate that assuming realistic heterogeneous elastic properties, a sufficiently deep fault geometry, and discarding any non-physical regularization of the inverse problem, we infer the SZU as caused by slip downdip of the main coseismic rupture.

Inconsistencies in the fit to vertical versus horizontal measurements have already been discussed for various subduction zones and processes. For instance, Klein et al. (2018) report an inconsistency in the amount of slow slip needed to fit horizontal versus vertical observations a few hundreds of km from the trench. Some postseismic slip models of the Maule event (e.g., Lin et al., 2013), or synthetic tests performed for an infinitely long megathrust (Hsu et al., 2006), report similar inconsistencies. It is common practice to discard or down-weight vertical data because of such inconsistencies and larger measurement errors. We show that by accounting for heterogeneities in elastic structure, we can reconcile vertical and horizontal observations.

With synthetic tests and a study of the 2010 M_w 8.8 Maule earthquake, we suggest that the SZU is likely caused by deep afterslip happening within the first hours following the mainshocks. For both the Maule and 2011 M_w 9.1 Tohoku earthquakes, the ambiguity of the SZU measurements highlights the difficulty to accurately evaluate the contribution of very early deformations occurring after large earthquakes (Twardzik et al., 2019). Our results advocate for the study of the postseismic phase as early as possible after the mainshock, as already emphasized by several authors (e.g., Twardzik et al., 2019; Ragon et al., 2019; Jiang et al., 2021).

While the occurrence of very early deep afterslip (hours after the mainshock, $\sim$100-km-deep) remains to be further investigated, it is coherent with a rate strengthening frictional behavior of the megathrust. For instance, numerical simulations of Muto et al. (2019); Barbot (2020) showed that stress-driven aseismic afterslip can occur at great depths (60-100-km-depth) by considering rate-and-state friction laws. Alternatively, viscous flow could also explain such early postseismic deformation (e.g., Montési & Hirth, 2003). Mallick et al. (2022) shown that power-law viscous flows are of greater amplitude at shorter time-scales for large earthquakes, what might explain why the SZU has only been observed for megathrust earthquakes. Rapid viscous flow is coherent with longer-term viscoelastic relaxation invoked for both the Maule and Tohoku earthquakes (e.g., Klein et al., 2016; Peña et al., 2020, 2021; Agata et al., 2019; Sun et al., 2014; Luo & Wang, 2021), but the similarity of surface displacements produced by afterslip or viscous flows prevents, at this stage, discriminating potential processes driving the SZU (e.g., Weiss et al., 2019; Mallick et al., 2022).

Acknowledgments

We thank Emilie Klein, an anonymous reviewer, and the associate editor for their excellent suggestions that help improved the original manuscript. We thank Rishav Mallick for fruitful discussions. MS was partially supported by the National Aeronautics and Space Administration under Grant No. 80NSSC19K1499.

Data and resources. Materials (without datasets) presented in this paper are archived and available on Zenodo, `doi.org/10.5281/zenodo.7120837`.
Static GNSS offsets for the 2010 Maule earthquake have been published in Vigny et al. (2011) and Lin et al. (2013). GNSS time series have been process by Klein et al. (2022), with data provided by Centro Sismolgico Nacional (CSN) of the Universidad de Chile (Báez et al., 2018), that can be retrieved from the GNSS database (`http://GNSS.csn.uchile.cl`).
GNSS time series for the 2011 Tohoku earthquake have been processed by Periollat et al. (2022). Static GNSS time series are accessible at `doi.org/10.17178/GNSS.products.Japan_GIPSYX.daily`. Such GNSS products are calculated and provided by the Institut of Sciences de la Terre (ISTerre), belonging to the Institut National des Sciences de l'Univers (INSU/CNRS) and the Observatoire des Sciences de lUnivers de Grenoble (OSUG / Universit Grenoble Alpes).
The Bayesian simulations were performed with the AlTar2 package (*AlTar, A Bayesian Framework for Inverse Problems*, 2022). The Classic Slip Inversion (CSI) Python library (Jolivet et al., 2014) developed by Romain Jolivet was used to build inputs for the Bayesian algorithm. The mesh for the FEM simulations was built using Coreform Cubit (*Coreform Cubit*, 2022). We used the finite-element code Pylith (Aagaard et al., 2013) to perform the simulations. Slab geometry, topography and crustal elastic properties from Slab2, LITHO1.0, and ETOPO1 models are available in Hayes et al. (2018); Pasyanos et al. (2014); NCEI (2008). 3D data were visualized using the open-source parallel visualization software ParaView/VTK (Ahrens et al., 2005). Figures were generated with the Matplotlib (Hunter, 2007) and Seaborn (Waskom, 2021) Python3 libraries.

References

Aagaard, B. T., Knepley, M. G., & Williams, C. A. (2013). A domain decomposition approach to implementing fault slip in finite-element models of quasi-static and dynamic crustal deformation. *Journal of Geophysical Research: Solid Earth*, *118*(6), 3059–3079. doi: 10.1002/jgrb.50217

Agata, R., Barbot, S. D., Fujita, K., Hyodo, M., Iinuma, T., Nakata, R., ... Hori, T. (2019). Rapid mantle flow with power-law creep explains deformation after the 2011 Tohoku mega-quake. *Nature Communications*, *10*(1), 1385. doi: 10.1038/s41467-019-08984-7

Ahrens, J., Geveci, B., & Law, C. (2005). 36 - ParaView: An End-User Tool for Large-Data Visualization. In C. D. Hansen & C. R. Johnson (Eds.), *Visualization Handbook* (pp. 717–731). Burlington: Butterworth-Heinemann. doi: 10.1016/B978-012387582-2/50038-1

AlTar, A Bayesian framework for inverse problems. (2022). v2.0, ParaSim Inc., California Institute of Technology. Available at github.com/lijun99/altar2-documentation.

Báez, J. C., Leyton, F., Troncoso, C., del Campo, F., Bevis, M., Vigny, C., ... Blume, F. (2018). The Chilean GNSS Network: Current Status and Progress toward Early Warning Applications. *Seismological Research Letters*, *89*(4), 1546–1554. doi: 10.1785/0220180011

Barbot, S. (2020). Frictional and structural controls of seismic super-cycles at the Japan trench. *Earth, Planets and Space*, *72*(1), 63. doi: 10.1186/s40623-020-01185-3

Bedford, J., Moreno, M., Baez, J. C., Lange, D., Tilmann, F., Rosenau, M., ... Vigny, C. (2013). A high-resolution, time-variable afterslip model for the 2010 Maule Mw = 8.8, Chile megathrust earthquake. *Earth and Planetary Science Letters*, *383*, 26–36. doi: 10.1016/j.epsl.2013.09.020

Coreform Cubit. (2022). v2022.4. Orem, UT: Coreform LLC. Retrieved from coreform.com.

Delouis, B., Nocquet, J.-M., & Vallée, M. (2010). Slip distribution of the February 27, 2010 Mw = 8.8 Maule Earthquake, central Chile, from static and high-rate GPS, InSAR, and broadband teleseismic data. *Geophysical Research Letters*, *37*(17). doi: 10.1029/2010GL043899

Hayes, G. P., Moore, G. L., Portner, D. E., Hearne, M., Flamme, H., Furtney, M., & Smoczyk, G. M. (2018). Slab2, a comprehensive subduction zone geometry model. *Science*, *362*(6410), 58–61. doi: 10.1126/science.aat4723

Hsu, Y.-J., Simons, M., Avouac, J.-P., Galetzka, J., Sieh, K., Chlieh, M., ... Bock, Y. (2006). Frictional Afterslip Following the 2005 Nias-Simeulue Earthquake, Sumatra. *Science*, *312*(5782), 1921–1926. doi: 10.1126/science.1126960

Hu, J., Li, Z. W., Ding, X. L., Zhu, J. J., & Sun, Q. (2013). Derivation of 3-D coseismic surface displacement fields for the 2011 Mw 9.0 Tohoku-Oki earthquake from InSAR and GPS measurements. *Geophysical Journal International*, *192*(2), 573–585. doi: 10.1093/gji/ggs033

Hunter, J. D. (2007). Matplotlib: A 2D Graphics Environment. *Computing in Science & Engineering*, *9*(3), 90–95. doi: 10.1109/MCSE.2007.55

Ichimura, T., Agata, R., Hori, T., Hirahara, K., Hashimoto, C., Hori, M., & Fukahata, Y. (2016). An elastic/viscoelastic finite element analysis method for crustal deformation using a 3-D island-scale high-fidelity model. *Geophysical Journal International*, *206*(1), 114–129. doi: 10.1093/gji/ggw123

Jiang, J., Bock, Y., & Klein, E. (2021). Coevolving early afterslip and aftershock signatures of a San Andreas fault rupture. *Science Advances*, *7*(15), eabc1606. doi: 10.1126/sciadv.abc1606

Jolivet, R., Duputel, Z., Riel, B., Simons, M., Rivera, L., Minson, S. E., ... Fielding, E. J. (2014). The 2013 Mw 7.7 Balochistan Earthquake: Seismic Potential of an Accretionary Wedge. *Bulletin of the Seismological Society of America*, *104*(2), 1020–1030. doi: 10.1785/0120130313

Kanamori, H. (1970). The Alaska Earthquake of 1964: Radiation of long-period surface waves and source mechanism. *Journal of Geophysical Research (1896-1977)*, *75*(26), 5029–5040. doi: 10.1029/JB075i026p05029

Klein, E., Duputel, Z., Zigone, D., Vigny, C., Boy, J.-P., Doubre, C., & Meneses, G. (2018). Deep Transient Slow Slip Detected by Survey GPS in the Region of Atacama, Chile. *Geophysical Research Letters*, *45*(22), 12,263–12,273. doi: 10.1029/2018GL080613

Klein, E., Fleitout, L., Vigny, C., & Garaud, J. (2016). Afterslip and viscoelastic relaxation model inferred from the large-scale post-seismic deformation following the 2010 Mw 8.8 Maule earthquake (Chile). *Geophysical Journal International*, *205*(3), 1455–1472. doi: 10.1093/gji/ggw086

Klein, E., Vigny, C., Nocquet, J.-M., & Boulze, H. (2022). A 20 year-long GNSS solution across South-America with focus in Chile. *Bulletin de la Société Géologique de France*, *193*(1), 5. doi: 10.1051/bsgf/2022005

Lange, D., Tilmann, F., Barrientos, S. E., Contreras-Reyes, E., Methe, P., Moreno, M., ... Beck, S. (2012). Aftershock seismicity of the 27 February 2010 Mw 8.8 Maule earthquake rupture zone. *Earth and Planetary Science Letters*, *317–318*, 413–425. doi: 10.1016/j.epsl.2011.11.034

Langer, L., Ragon, T., Sladen, A., & Tromp, J. (2020). Impact of topography on earthquake static slip estimates. *Tectonophysics*, 228566. doi: 10.1016/j.tecto.2020.228566

Lay, T. (2017). A review of the rupture characteristics of the 2011 Tohoku-oki Mw 9.1 earthquake. *Tectonophysics*. doi: 10.1016/j.tecto.2017.09.022

Lay, T., Kanamori, H., Ammon, C. J., Koper, K. D., Hutko, A. R., Ye, L., … Rushing, T. M. (2012). Depth-varying rupture properties of subduction zone megathrust faults. *Journal of Geophysical Research: Solid Earth*, *117*(B4). doi: 10.1029/2011JB009133

Li, S., Moreno, M., Bedford, J., Rosenau, M., Heidbach, O., Melnick, D., & Oncken, O. (2017). Postseismic uplift of the Andes following the 2010 Maule earthquake: Implications for mantle rheology. *Geophysical Research Letters*, 2016GL071995. doi: 10.1002/2016GL071995

Lin, Y.-n. N., Sladen, A., Ortega-Culaciati, F., Simons, M., Avouac, J.-P., Fielding, E. J., … Socquet, A. (2013). Coseismic and postseismic slip associated with the 2010 Maule Earthquake, Chile: Characterizing the Arauco Peninsula barrier effect. *Journal of Geophysical Research: Solid Earth*, *118*(6), 3142–3159. doi: 10.1002/jgrb.50207

Lorito, S., Romano, F., Atzori, S., Tong, X., Avallone, A., McCloskey, J., … Piatanesi, A. (2011). Limited overlap between the seismic gap and coseismic slip of the great 2010 Chile earthquake. *Nature Geoscience*, *4*(3), 173–177. doi: 10.1038/ngeo1073

Luo, H., & Wang, K. (2021). Postseismic geodetic signature of cold forearc mantle in subduction zones. *Nature Geoscience*, *14*(2), 104–109. doi: 10.1038/s41561-020-00679-9

Luttrell, K., Tong, X., Sandwell, D., Brooks, B., & Bevis, M. (2011). Estimates of stress drop and crustal tectonic stress from the 27 February 2010 Maule, Chile, earthquake: Implications for fault strength [Journal Article]. *Journal of Geophysical Research B: Solid Earth*, *116*(11). doi: 10.1029/2011JB008509

Mai, P. M., & Thingbaijam, K. K. S. (2014). SRCMOD: An Online Database of Finite-Fault Rupture Models. *Seismological Research Letters*, *85*(6), 1348–1357. doi: 10.1785/0220140077

Mallick, R., Lambert, V., & Meade, B. (2022). On the Choice and Implications of Rheologies That Maintain Kinematic and Dynamic Consistency Over the Entire Earthquake Cycle. *Journal of Geophysical Research: Solid Earth*, *127*(9), e2022JB024683. doi: 10.1029/2022JB024683

Minson, S. E., Simons, M., & Beck, J. L. (2013). Bayesian inversion for finite fault earthquake source models I – theory and algorithm. *Geophysical Journal International*, *194*(3), 1701–1726. doi: 10.1093/gji/ggt180

Montési, L. G. J., & Hirth, G. (2003). Grain size evolution and the rheology of ductile shear zones: From laboratory experiments to postseismic creep. *Earth and Planetary Science Letters*, *211*(1), 97–110. doi: 10.1016/S0012-821X(03)00196-1

Moreno, M., Melnick, D., Rosenau, M., Baez, J., Klotz, J., Oncken, O., … Hase, H. (2012). Toward understanding tectonic control on the Mw 8.8 2010 Maule Chile earthquake. *Earth and Planetary Science Letters*, *321–322*, 152–165. doi: 10.1016/j.epsl.2012.01.006

Muto, J., Moore, J. D. P., Barbot, S., Iinuma, T., Ohta, Y., & Iwamori, H. (2019). Coupled afterslip and transient mantle flow after the 2011 Tohoku earthquake. *Science Advances*, *5*(9), eaaw1164. doi: 10.1126/sciadv.aaw1164

NCEI, N. C. f. E. (2008). *ETOPO1 1 Arc-Minute Global Relief Model.* https://www.ncei.noaa.gov/access/metadata/landing-page/bin/iso?id=gov.noaa.ngdc.mgg.dem:316.

Obara, K., & Kato, A. (2016). Connecting slow earthquakes to huge earthquakes. *Science*, *353*(6296), 253–257. doi: 10.1126/science.aaf1512

Ortega-Culaciati, F., Simons, M., Ruiz, J., Rivera, L., & Díaz-Salazar, N. (2021). An EPIC Tikhonov Regularization: Application to Quasi-Static Fault Slip Inversion. *Journal of Geophysical Research: Solid Earth*, *126*(7), e2020JB021141.

doi: 10.1029/2020JB021141

Ozawa, S., Nishimura, T., Suito, H., Kobayashi, T., Tobita, M., & Imakiire, T. (2011). Coseismic and postseismic slip of the 2011 magnitude-9 Tohoku-Oki earthquake. *Nature*, *475*(7356), 373–6.

Pasyanos, M. E., Masters, T. G., Laske, G., & Ma, Z. (2014). LITHO1.0: An updated crust and lithospheric model of the Earth. *Journal of Geophysical Research: Solid Earth*, *119*(3), 2153–2173. doi: 10.1002/2013JB010626

Peña, C., Heidbach, O., Moreno, M., Bedford, J., Ziegler, M., Tassara, A., & Oncken, O. (2020). Impact of power-law rheology on the viscoelastic relaxation pattern and afterslip distribution following the 2010 Mw 8.8 Maule earthquake. *Earth and Planetary Science Letters*, *542*, 116292. doi: 10.1016/j.epsl.2020.116292

Peña, C., Heidbach, O., Moreno, M., Melnick, D., & Oncken, O. (2021). Transient Deformation and Stress Patterns Induced by the 2010 Maule Earthquake in the Illapel Segment. *Frontiers in Earth Science*, *9*, 157. doi: 10.3389/feart.2021.644834

Periollat, A., Radiguet, M., Weiss, J., Twardzik, C., Amitrano, D., Cotte, N., . . . Socquet, A. (2022). Transient Brittle Creep Mechanism Explains Early Postseismic Phase of the 2011 Tohoku-Oki Megathrust Earthquake: Observations by High-Rate GPS Solutions. *Journal of Geophysical Research: Solid Earth*, *127*(8), e2022JB024005. doi: 10.1029/2022JB024005

Plafker, G. (1965). Tectonic Deformation Associated with the 1964 Alaska Earthquake: The earthquake of 27 March 1964 resulted in observable crustal deformation of unprecedented areal extent. *Science*, *148*(3678), 1675–1687. doi: 10.1126/science.148.3678.1675

Plafker, G., & Savage, J. C. (1970). Mechanism of the Chilean Earthquakes of May 21 and 22, 1960. *GSA Bulletin*, *81*(4), 1001–1030. doi: 10.1130/0016-7606(1970)81[1001:MOTCEO]2.0.CO;2

Pollitz, F. F., Brooks Ben, Tong Xiaopeng, Bevis Michael G., Foster James H., Bürgmann Roland, . . . Blanco Mauro (2011). Coseismic slip distribution of the February 27, 2010 Mw 8.8 Maule, Chile earthquake. *Geophysical Research Letters*, *38*(9). doi: 10.1029/2011GL047065

Ragon, T., & Simons, M. (2021). Accounting for uncertain 3-D elastic structure in fault slip estimates. *Geophysical Journal International*, *224*(2), 1404–1421. doi: 10.1093/gji/ggaa526

Ragon, T., Sladen, A., Bletery, Q., Vergnolle, M., Cavalié, O., Avallone, A., . . . Delouis, B. (2019). Joint Inversion of Coseismic and Early Postseismic Slip to Optimize the Information Content in Geodetic Data: Application to the 2009 Mw6.3 L'Aquila Earthquake, Central Italy. *Journal of Geophysical Research: Solid Earth*, *124*(10), 10522–10543. doi: 10.1029/2018JB017053

Rietbrock, A., Ryder, I., Hayes, G., Haberland, C., Comte, D., Roecker, S., & Lyon-Caen, H. (2012). Aftershock seismicity of the 2010 Maule Mw=8.8, Chile, earthquake: Correlation between co-seismic slip models and aftershock distribution? *Geophysical Research Letters*, *39*(8). doi: 10.1029/2012GL051308

Ruegg, J. C., Rudloff, A., Vigny, C., Madariaga, R., de Chabalier, J. B., Campos, J., . . . Dimitrov, D. (2009). Interseismic strain accumulation measured by GPS in the seismic gap between Constitución and Concepción in Chile. *Physics of the Earth and Planetary Interiors*, *175*(1), 78–85. doi: 10.1016/j.pepi.2008.02.015

Ruiz, S., & Madariaga, R. (2018). Historical and recent large megathrust earthquakes in Chile. *Tectonophysics*, *733*, 37–56. doi: 10.1016/j.tecto.2018.01.015

Savage, J. C. (1983). A dislocation model of strain accumulation and release at a subduction zone. *Journal of Geophysical Research: Solid Earth*, *88*(B6), 4984–4996. doi: 10.1029/JB088iB06p04984

Sun, T., Wang, K., Iinuma, T., Hino, R., He, J., Fujimoto, H., . . . Hu, Y. (2014). Prevalence of viscoelastic relaxation after the 2011 Tohoku-oki earthquake.

Nature, *514*(7520), 84–87. doi: 10.1038/nature13778
Twardzik, C., Vergnolle, M., Sladen, A., & Avallone, A. (2019). Unravelling the contribution of early postseismic deformation using sub-daily GNSS positioning —. *Scientific Reports*, *9*(1), 1775. doi: 10.1038/s41598-019-39038-z
van Dinther, Y., Preiswerk, L. E., & Gerya, T. V. (2019). A Secondary Zone of Uplift Due to Megathrust Earthquakes. *Pure and Applied Geophysics*, *176*(9), 4043–4068. doi: 10.1007/s00024-019-02250-z
Vigny, C., Socquet, A., Peyrat, S., Ruegg, J.-C., Métois, M., Madariaga, R., ... Kendrick, E. (2011). The 2010 Mw 8.8 Maule Megathrust Earthquake of Central Chile, Monitored by GPS. *Science*, *332*(6036), 1417–1421. doi: 10.1126/science.1204132
Waskom, M. L. (2021). Seaborn: Statistical data visualization. *Journal of Open Source Software*, *6*(60), 3021. doi: 10.21105/joss.03021
Weiss, J. R., Qiu, Q., Barbot, S., Wright, T. J., Foster, J. H., Saunders, A., ... Echalar, A. (2019). Illuminating subduction zone rheological properties in the wake of a giant earthquake. *Science Advances*, *5*(12), eaax6720. doi: 10.1126/sciadv.aax6720
Xiong, L., Xu, C., Liu, Y., Zhao, Y., Geng, J., & Ortega-Culaciati, F. (2022). Three-dimensional displacement field of the 2010 Mw 8.8 Maule earthquake from GPS and InSAR data with the improved ESISTEM-VCE method. *Frontiers in Earth Science*, *10*.
Yue, H., Lay, T., Rivera, L., An, C., Vigny, C., Tong, X., & Báez Soto, J. C. (2014). Localized fault slip to the trench in the 2010 Maule, Chile Mw = 8.8 earthquake from joint inversion of high-rate GPS, teleseismic body waves, InSAR, campaign GPS, and tsunami observations. *Journal of Geophysical Research: Solid Earth*, *119*(10), 7786–7804. doi: 10.1002/2014JB011340